Micro-Stratigraphical Investigation on Corrosion Layers in Ancient Bronze Artefacts of Urartian Period by Scanning Electron Microscopy, Energy-Dispersive Spectrometry, and Optical Microscopy

Yeghis Keheyan [1],* and Giancarlo Lanterna [2]

[1] SMATCH-Scientific Methodologies Applied to Cultural Heritage, c/o Department of Chemistry, University of Rome "La Sapienza", P.le Aldo Moro, 5, 00185 Rome, Italy

[2] Opificio delle Pietre Dure e Laboratori di Restauro, Viale Filippo Strozzi 1, 50129 Florence, Italy; giancarlo.lanterna@beniculturali.it

* Correspondence: yeghis.keheyan@uniroma1.it

Abstract: The results of the analysis on some fragments of bronze belts and a bowl discovered from southwestern Armenia at the Yegheghnadzor archaeological site are discussed. The samples are dated to the 7–6th millennium BCE from the Urartian period. The artefacts were corroded, and a multilayer structure was formed. To study the stratigraphy of layers and their composition, the samples have been analyzed using SEM-EDS (Scanning Electron Microscopy, Energy-Dispersive Spectrometry) and OM (Optical Microscopy) techniques. The bronze finds appear with the typical incrustations rich in alloy alteration compounds. Concentrations of copper and tin in the alloys were quantified by SEM-EDS: the pattern and the percentage of the alloy are the same for the belts. Regarding the bowl sample, it is constituted by two foils perfectly in contact but different in color, thickness, and composition. The results evidenced that only two elements participate in forming the alloy composition in the samples: Cu and Sn. The tin content is variable from 7.75% to 13.56%. Other elements such as Ag, As, Fe, Ni, P, Pb, Sb, and Zn make up less than 1% and can be considered as impurities.

Keywords: bronze belts; bowl; SEM-EDS; OM; Urartu

1. Introduction

During the Bronze Age, Armenia was an integral part of a cultural zone between the Van, Urmia, and Sevan lakes, with contacts mainly toward the Near East. It is clear that metals were a very essential factor both for the definition of inner values of the considered society and for its outer connections: from this perspective, the active southern relations of the region can be interpreted mainly as based on the metal factor. The authors of [1,2] report that metallurgy in the Southern Caucasus and Armenia in particular appears with the extraction of native copper and cold working-cum-annealing at the beginning of the 6th millennium BC. The study and understanding of manufacturing technologies and alteration phenomena of archaeological bronze artifacts are of great importance in the field of conservation and restoration [3]. The elemental composition of a bronze alloy represents important information to archaeologists because it can provide a clue on the technology used for the production of the object and be a reference to its age and provenance. The characterization of an alloy should be always coupled to the analysis of patina, especially for archaeological bronzes, which show peculiar morphology and composition and can hardly be falsified. Depending on the environment of exposure (underground, atmospheric, marine), bronze alloys form different corrosion products such as hydrated copper carbonates, sulfates, sulfides, chlorides, oxides, oxalates, as well as those resulting from other alloying elements, such as tin and lead. Artifacts made of copper,

iron, or other metals and alloys are very common in archaeology [4–7]. In particular, bronze artifacts were extensively used in the past and their corrosion process uncovered in the burial condition was of great interest among researchers in the last years; see [8]. Several bronze belts were founded in Armenia due to archaeological excavations or accidentally. There are quite controversial opinions among the researchers concerning the dating of these belts [9–14]. The culture for these belts originates in the 14th century B.C. and continues during the existence of Urartian State expansion (until 7–6th centuries B.C.). There are various views on the functions that these bronze belts have performed; however, it is considered mainly as the part of warrior's defensive outfit, the continuation of the armor. In any case, these belts were able to afford only the representatives of higher authoritative and cleric strata. According to their thematic scenes, they are divided into different classes: hunting, military, mythological, genre, and elemental movement. There are belts with only geometric ornaments and unornamented ones. Examples of this art are fragments of corroded belts found in the cemetery of Yegheghnadzor (Armenia). The belts are confined by two edge lines of parallel relief. Edges are prepared with holes to be fixed on the leather. The façade, including the border, is engraved with different figures as was used for Bianili's (Urartu) belts, in two directions: one part from left to right and the other from right to left (Figure 1). Belt. 1, N° catalogue: 4112, Height: 10 cm, Length: approximately 80–100 cm, Thickness: 0.1 cm.
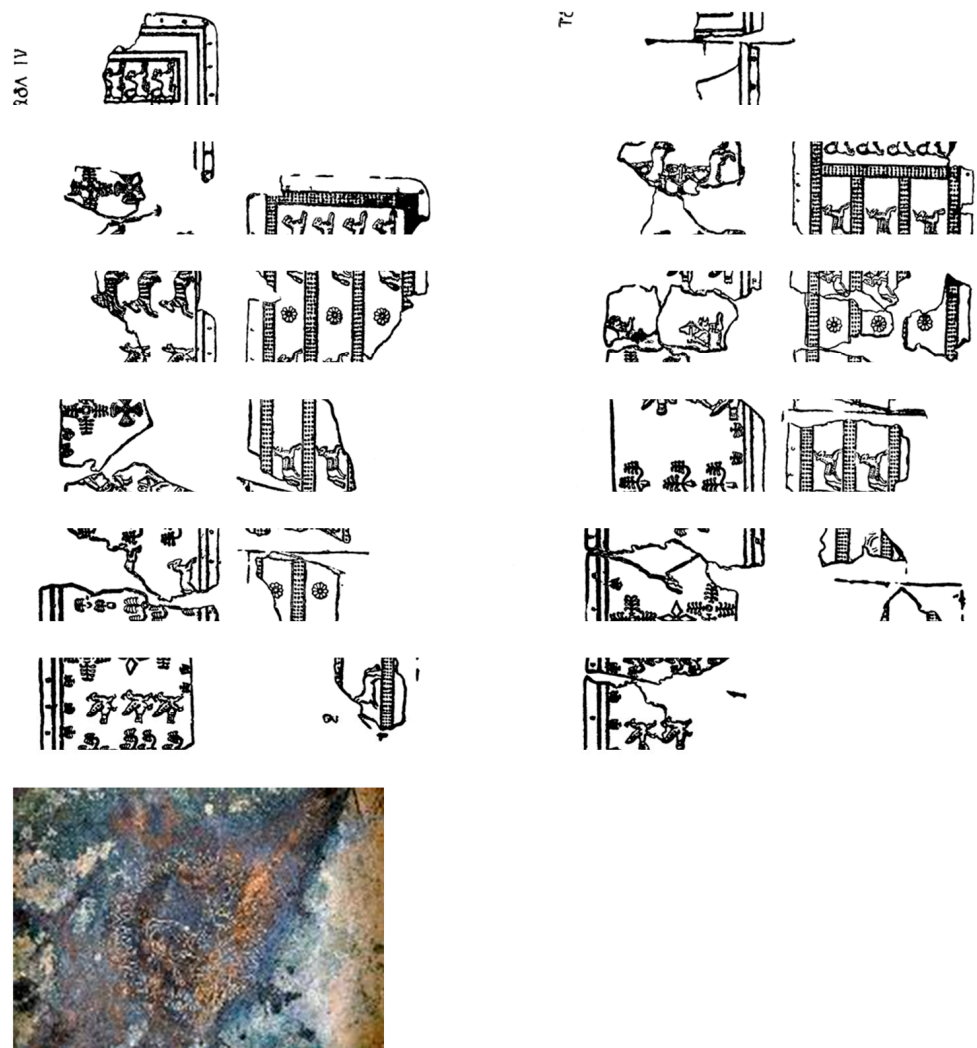

Figure 1. Belts 1 and 2 (above) and below bowl.

Thirty-one fragments of the decorated bronze belts have been put back together to recreate a realistic hypothesis of what the belt would have been. All the decorations of the belt are embossed, as can be seen from the back of some fragments of the object. The belts were framed with lines by regularly spaced holes. Under these holes, there are two *in relief* straight lines that run along all the perimeter of the belt, and there is a decoration that consists of a stripe of regular spaced small trees made of frequent short lines representing the base, the trunk, and eight branches. Bronze belt (2) N° catalogue: 4111, Height: 10.5 cm, Length: not calculable, Thickness: 0.1 cm. Judging from the preserved part of the belt, the strips feature scenes of trees of life, rosettes, and crosses and are divided into some hunting scenes.

Decorated bronze vessel, N° catalogue: 1304/4110, Diameter: 19 cm, Thickness: 0.1 cm.

The decorated bronze vessel, in the shape of a shallow bowl, is almost completely preserved. Some points of the base are corroded, and the body is broken in two spots. The rim has the same width as the rest of the vessel, slightly everted, and it starts from a swelling of the body: it can be seen clearly on the right side of the vessel, which is better preserved. The base is not perfectly flat; instead, it is rather convex. On the lower right side of the base, there are two holes at a distance of about 1 cm one from the other: the left one is made 1.6 cm from the rim, while the right one can be seen 1.1 cm from the rim. Archaeometallurgical investigations in Armenia during the post-Soviet period entered a completely new stage with the application of modern analytical methods such as X-ray fluorescence analysis (XRF), instrumental neutron activation analysis (INAA), Scanning Electron Microscope with Electron Probe Micro Analyses (SEM-EPMA), and Inductively Coupled Plasma-Mass Spectrometry (ICP-MS) to study metal artifacts and ores, and researchers have been created a large database of chemical compositions and lead isotope analyses of artifacts. This is based on data from new excavations and a review of previous work. Geochemical and lead isotope analyses of ores in some cases enable metal provenance definitions [14–17]. The study of metal findings of the cemetery of Yegheghnadzor was based on both morphological and mineral phase analyses of patinas and metals. These pieces show that the formation of patina and its chemical and structural features are largely influenced by the chemical composition and the metallurgical features of the alloy as well as by the context characteristics. In particular, to be sure of the metal alloys' components, micro-samples of the metal sheets were used in the form of cross-sections, which were analyzed stratigraphically. It is crucial to study micro-stratification in finds such as excavation because corrosion patina, concretions, and their cross products make it very complex to define the metal percentages of the alloys. In the recent past, some of the authors have already come across very precise data obtained from a destructive analysis (ICP) of bronze chips, which then turned out to be completely misleading due to the considerable redistribution of the alloy elements, especially near the surfaces. The analysis of unaltered areas carried out at SEM/EDS, even if less accurate, revealed a very different but reliable bronze composition [14].

2. Experimental Conditions

For this work, both archaeological and experimental traces were observed and defined. The analytical approach took place first by observing the fragments with a stereomicroscope photographing them on a grid of graph paper, both on one side and the other. By convention, considering the fragments as caps, the front face was considered the external surface, the convex one, while the concave face was considered the rear surface. The thickness of each fragment was observed as well, positioning the profile of each one in a sand bed to show the whole stratification. The surfaces and the profiles of the fragments were observed at various magnifications (0.8×–16×) and photographed with the Leica digital camera. From each fragment, a micro-sample including the entire thickness (bulk metal, patinas, and concretions) was taken; it was embedded in polyester resin (Mecaprex) and subsequently ground and polished transversely to obtain a cross-section. The samples were observed with a Zeiss Axioplan 2 optical microscope equipped with halogen (Osram

100W) and ultraviolet (Zeiss Colibri UV LED, 360 nm) light sources and objectives Epifluar with 10× to 50× magnification; the images were recorded with a Canon EOS 1000 camera with 16 Mpx sensor and the Canon image Browser acquisition software. Subsequently, the same cross-sections were mounted on Al stubs (Ø = 13 mm) with a conductive adhesive based on metallic Ag (Agar silver paint) and metalized by a graphite sputter (Agar scientific sputter-coater, ca 40 mA), observing and analyzing them in high-vacuum SEM. EDX analyses were performed using a microprobe. The elements analysis was carried out employing an EDS microprobe Oxford "X-Max 80 Silicon Drift Detector" (SDD), and the analytic results, both in the form of XRF spectra of spots or areas and the distribution maps of the main elements, were processed using the Oxford "AZTEC 2.0" software.

3. Results and Discussions

The first fragment comes from the belt n.1 and has a triangular shape as well as two faces with a slight complementary curvature: the concave face was considered internal, while the convex one was considered external: on the inner face, there are extended dark reddish-brown concretions, while on the outermost face, there are more yellowish concretions.

The bronze sample appears with the typical incrustations rich in alloy alteration compounds. Concentrations of copper and tin in the alloys were quantified by SEM-EDS: the type and the percentage of the alloy are the same for the belts. Concerning the bowl, it is constituted by two foils that are perfectly in contact but different in color, thickness, and composition.

The results determine that only two elements play the main role to form alloy composition in the samples: Cu and Sn. The tin content is variable from 7.75 to 13.56% and it cannot be considered as an alloying pattern based on Sn. Other elements such as Ag, As, Fe, Ni, P, Pb, Sb, and Zn globally are lower than 1% in many samples and do not play an important role in the alloying process. They can be considered as impurities that may originate from mother stone ores. In Figure 2 illustrated three fragments, in front and rear sides.
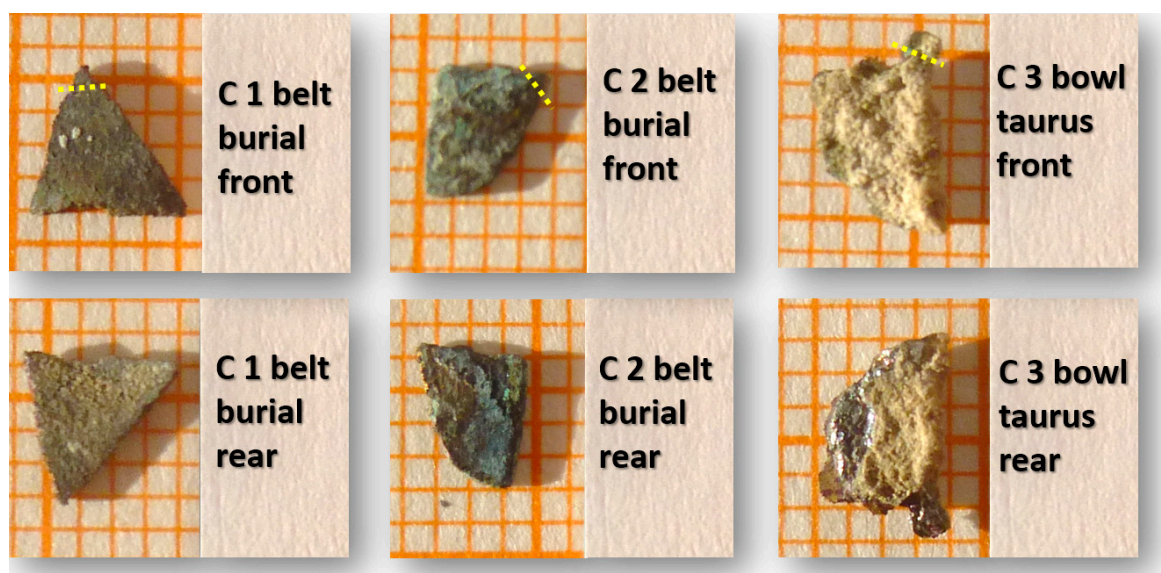

Figure 2. Macro-photos of three metal fragments: C1 and C2 from a belt buckle, C3 from a bowl. Conventionally, the convex part is attributed to the frontal face (1 box = 1 mm). Yellow line: micro-sample cut edge.

The whole fragments were placed on a support and were also observed transversally to make its thickness visible where it is possible to perceive metallic layers of yellowish appearance (Figure 3): at a higher magnification, they show the morphology and grain of the concretion through which both the oxide patina and the parts of metal with a yellowish, almost golden appearance can be seen.
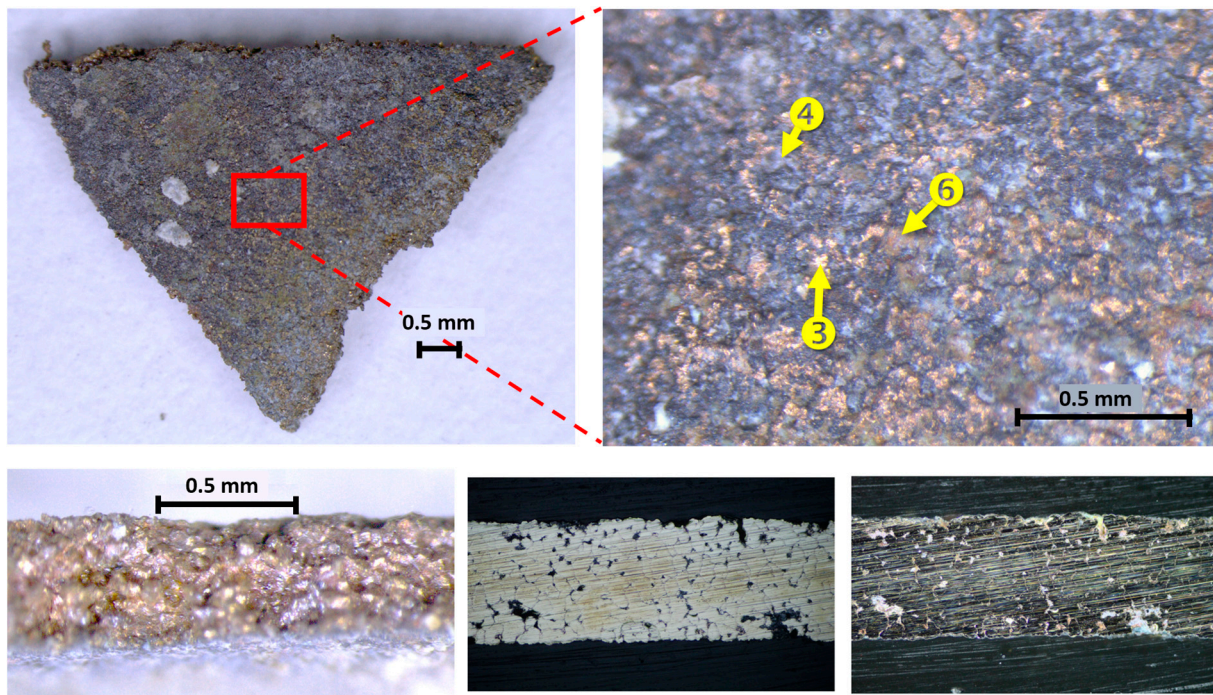
Figure 3. Above from left to right; C1 front macro photo with red box detail, C1 front stereomicroscope detail of the surface morphology and EDX spot positions in the main three different colors; (below) thickness macro photo, cross-section micro photo (dark field, center, bright field, left).

Being a metal sample, thus an electric conductor, it was placed as is on a 13 mm aluminum stub by means of a conductive carbon tape and was observed with SEM without needing to treat it beforehand with surface coatings. The SEM observation was performed with the primary electron detector (BSE, back-scattered electrons, in the images taken at the SEM, are marked QBSD) which allows observing, in addition to the morphology, also the distribution of the elements present or the density of the crystalline phases: heavy elements appear progressively brighter, while light elements are always darker in proportion to their atomic number. i.e., C (typical of organic materials) appears black, while Pb and Au appear white; phases as dense as silicates appear darker than quartz (silicon dioxide much more compact): at SEM (Figure 4), there are parts containing elements with lower atomic numbers, typical of concretions, containing Fe and Si and where they just transpose Cu and Sn of bronze and the underlying patina: among the medium and low atomic weight elements, we can see the distribution of the yellow concretions in a darker tone and the metal matrix, light gray, with some grains much lighter.

Using the differentiation enhanced by the BSE detector, elemental analyses were performed punctually both on the concretions, on the patinas, and the uncovered metal areas. Initially, SEM-BSE micrographs of corrosion layers show different stratigraphic sequences and exhibit differences between chemical composition and phases that form corrosion morphology in samples. To identify the chemical composition of the layers, SEM-EDS analyses are performed on each specific layer. The main elements detected in layers are Cu, Sn, Cl, and O. The Cu and Sn amounts are variable, and when the amount of Sn increases, the Cu decreases. In contrast, chlorine and oxygen were detected at variable levels in almost all layers.
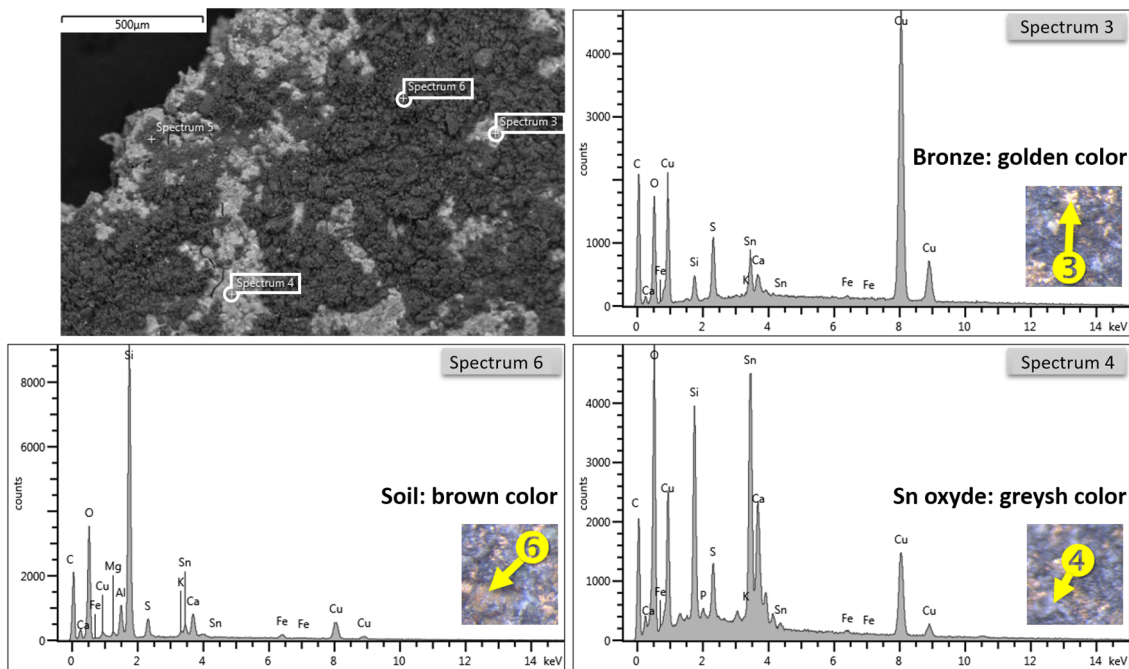
Figure 4. SEM/BSE image of the C1 surface detail with three analytical EDX spots: sp3 = bronze alloy (golden color), sp4 = tin oxide (grayish color), sediment and alteration products, sp6 (brown color), crust of sediments of the excavated soil.

On the other side, there are still oxygen and elements belonging to the oxidized phases of the metal: the spectrum number six in Figure 4 shows the average composition of the patina and is a concretion based mainly on silicates containing also some aluminum; these concretions are phases of more or less hydrated ferrous aluminosilicates that differ slightly in color in the concretions of the two faces: the inner face is more yellow because it has a higher iron content than the outer face.

In Figure 5, the cross-section analysis of C1 shows the status of the bronze alloy.

The image in SEM with BSE shows that the alloy is apparently in a good state of conservation; the intergranular profiles of the bronze and some rounded inclusions that appear dark gray are still visible; plus, there are also other inclusions that follow the intergranular profile with a slightly lighter tone than the previous one. The punctual EDX analyses carried out on the three different types show the simple composition of the bronze alloy, with high copper content and without other metal elements (As, Sb, Pb). The rounded inclusions sometimes have a metallic trace of O_2 in copper. Most likely (Lošinj athlete bronzes) [18] as reported for other archaeological bronzes, native copper was found due to the reduction of oxidized copper of the alloy. The other (sp30) linear inclusions are based on SnO_2 probably also deriving from precipitation in the intergranular spaces of the oxidized tin of the alloy.

In Figure 6, a detail in BSE is given at the higher magnification of the alloy bulk where two areas of the metallic bulk with different compositions of the elements are evident: the lighter part indicates the alpha phase of the alloy where the percentages of copper and tin are respectively detectable (88% and 11%), while the darker area contains in addition to the micro-cavities with sediment (visible in black) alloying metals, oxygen, sulfur, and chlorine, as well as some agents of bronze oxidation.
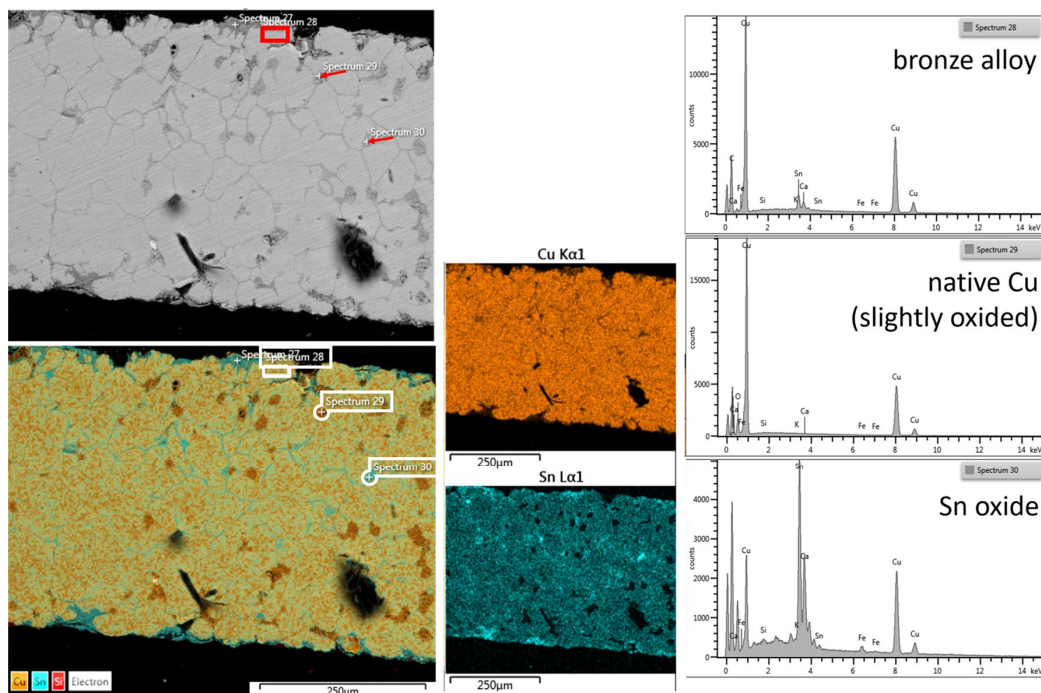
Figure 5. (left column to right): SEM/BSE image of the C1 cross-section with the mark of EDX analyses, EDX color map of the principal elements reconstructed overlapping the BSE image; EDX distribution maps of the single elements Cu and Sn; EDX spectra: composition of the bulk alloy (sp 28), the grains are more visible, spaced, and filled with tin oxide (sp 30); tin oxide is already present near the contour of the cross-section; pure Cu or slightly oxidized grows into small spaces inside the alloy (sp 29).
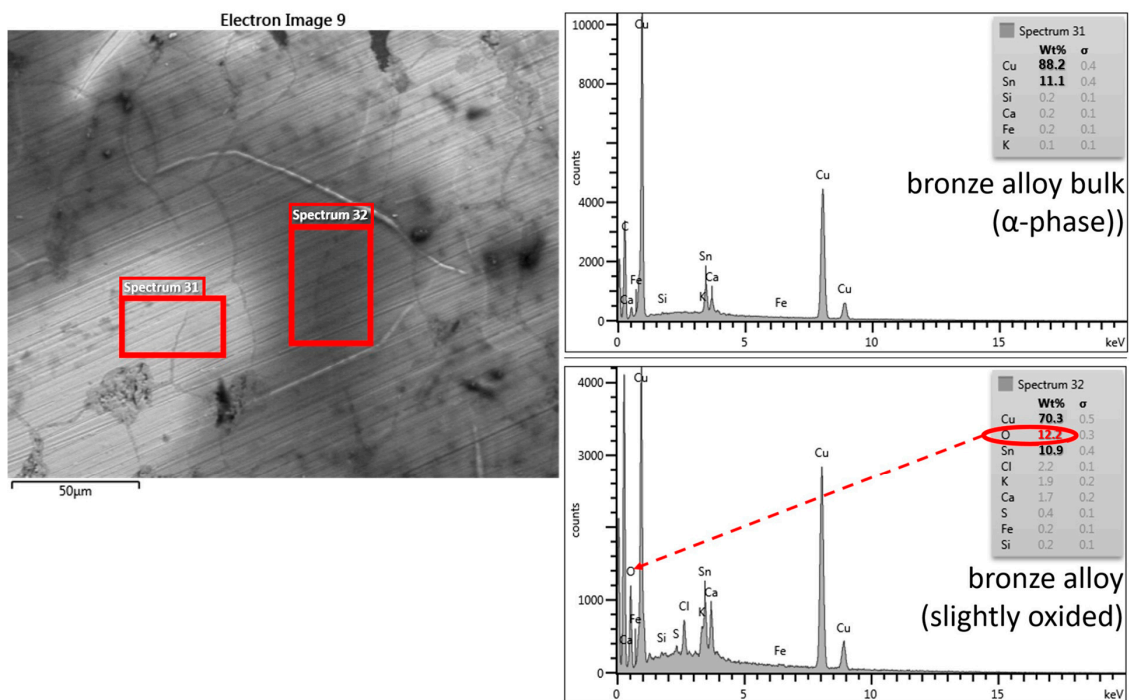

Figure 6. SEM/BSE image of the C1 cross-section: bulk alloy; some grain profiles are visible, different cavities with sediment inclusion (black), and some oxidation phenomena (medium gray). The boxes are relative to two different alloy phases: sp31 = α phase bronze alloy, sp32 = bronze alloy slightly oxidized.

In particular, there are white densities in which the metal alloy appears much richer in Sn (sp1 Figure 7, below, similar to sp 27 in Figure 5), probably indicating a rich phase in the element or a point of attack of tin by external degradation agents.
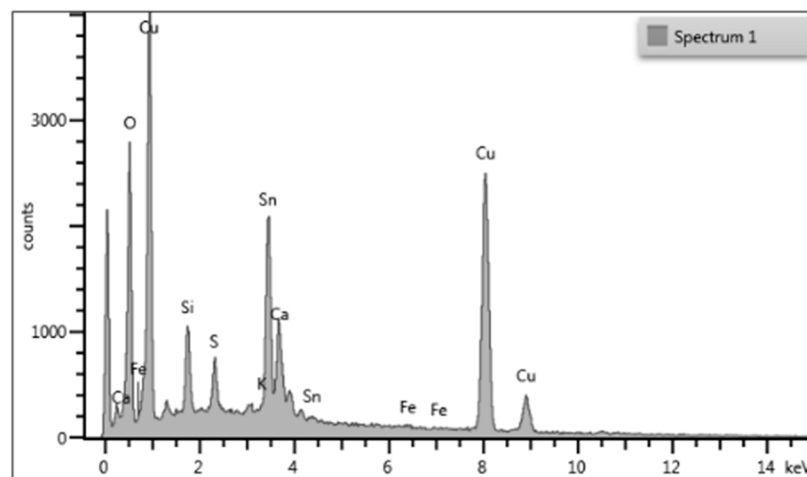

Figure 7. EDX spectrum of a bright area in the bulk alloy, tin and oxygen are related as copper and sulfur.

Then, a very small portion of the fragment, including all its thickness, was embedded into polyester resin to obtain a cross-section, which is useful to observe the true stratigraphy under the photomicroscope [1]. The halogen illumination source was used both with the dark field technique and the bright field technique; in the first case, there is an exact perception of the color of both the metals and the patinas or concretions, whereas the bright field allows observing the reflection of the smoothed granules and therefore highlights the different specularity of the intact granules to the corroded ones or the incoherent materials present in intergranular spaces. The lamina has a very regular thickness, approximately 1500 μm, and it is formed by a fairly homogeneous and compact metal in which the granulation is barely visible in the bright field, which is rather more evident near the two outer and inner surfaces, where the oxidation has accentuated the distance between the granules, sometimes filling it with residues of alloy oxidation material.

Sample 2 (C2) in Figure 8 is a fragment with very thick (>200 μm) oxidation patinas on both sides.

The fragment was investigated at the different colors and thicknesses: a stereomicroscope observation reveals that the patina is well adherent to the metal of reddish-brown, purplish colors and the thicker light gray surface is discontinuous, indicating fouling. The SEM analysis of the sample shows that the thicker part is also the one with the darker gray tone in BSE, the less dense, which is probably related to the earthy mineral phases based mainly on silicon and aluminum compounds. The long-term exposure that objects achieve in their environments through a steady-state regime has implicitly induced the thickness of the ancient bronze patinas, but it is not a function of the exposure time.

A buried metal dynamically generates a patina, sometimes leading to the complete disintegration of the metal (ferrous alloys), or, as in the case of copper alloys, up to a certain thickness, which makes the system stable. In general, the patinas can be classified into two main types: those that preserve the demarcation with the original surface and those that instead corrode and break up the profile of the product. Simplified examples of this subdivision are reported in the literature [19–22]. Patinas resulting from redox processes are attributable to the first type; crusts and patinas are also generated by acid–base reactions related to the second in which moisture flows play a central role in the transport of ions (i.e., mainly through hydrolysis and ionic exchange), while a third type includes those deriving from processes of site contamination (diffusion, segregation, deposition, etc.). These deposits/products are formed at different stages and are characteristic of

specific types of patina, i.e., oxides and sulfides, formed since the utilization period, which constitute the primary patina. Halogenides, oxyhydroxides, carbonates, sulfates, phosphates, etc., which formed in the final period of utilization (i.e., before abandonment) and the first stage of the lying period help to define the secondary patina. Finally, the phases resulting from the physical processes of diffusion, segregation, deposition, and recrystallization constitute the so-called patina of contamination. For artifacts or minerals containing pure copper, it should be remembered that the corrosion products of this element formed in natural or artificial conditions often manifest themselves with similar colors: red for Cu (I) oxide, with shades from green to blue for Cu (II) compounds, etc.
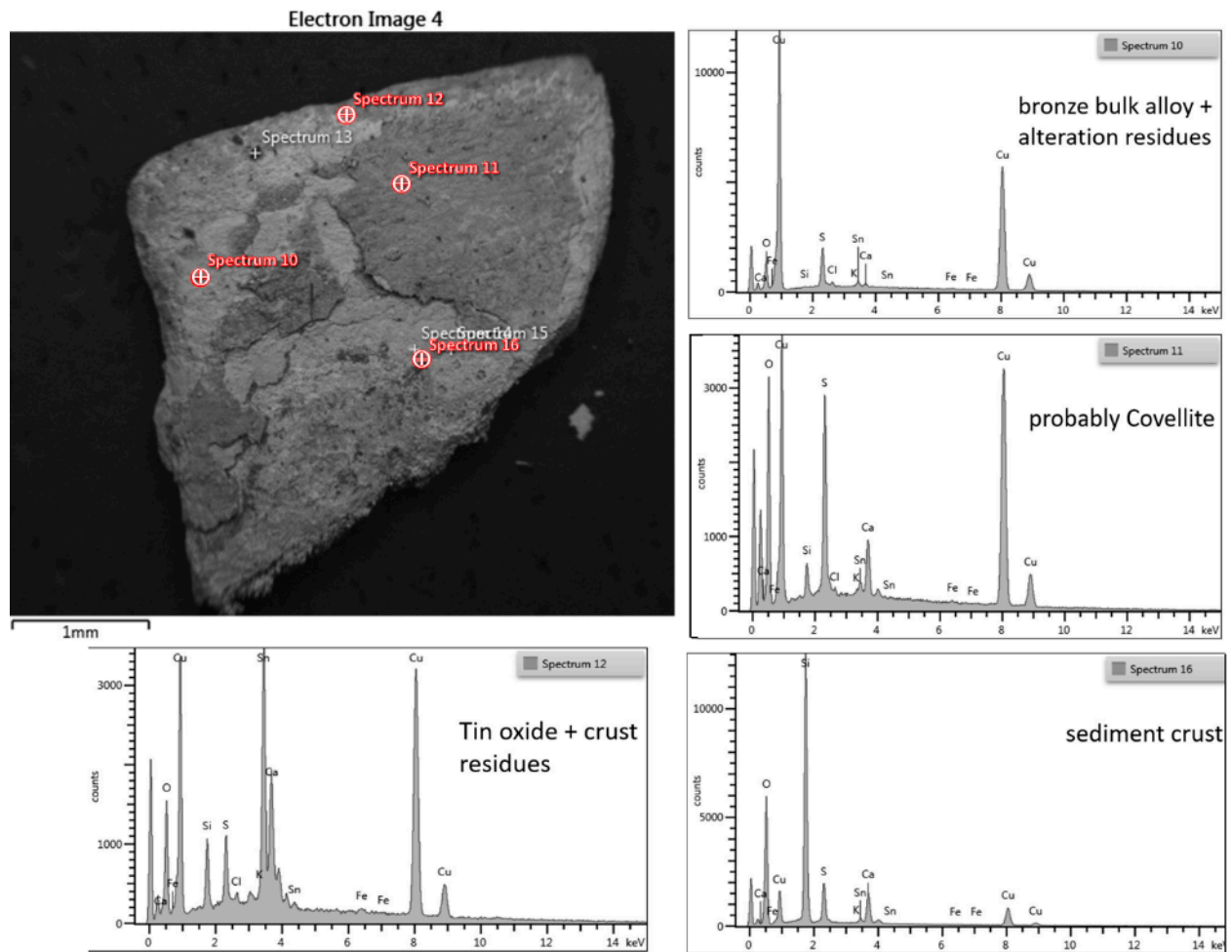

Figure 8. Front side SEM/BSE image of the encrusted surface with the position of EDX analyses spot and the relative EDX spectra showing the hypothesized composition.

The patina colors are directly connected to the nature of the corrosive environment and not to the composition of the bronze alloys, as reported by [23,24]. If patinas stay for a long time in contact with soil, its color changed from gray to dark green, to green, and to blue. The dark green patina is characteristic of an organic coating with a coloration treatment, covering mineral grains poorly coalesced, which are not the consequences of natural corrosion. Thepatina more in relief and less dense has in the composition a high percentage of Sn (sp 12 and 14, Figure 8), which justifies the light color as Sn oxide; the purplish patina contains mostly copper and sulfur, which are elements that suggest the presence of covellite (copper sulfide, purplish) and greenish copper hydroxyl sulfate (typically antlerite or brochantite), which together with the dark red patina composed of the red cuprite (Cu_2O) and dark tenorite (CuO) copper oxides give the general brownish

tone to the patina; together with the mentioned elements, there are also calcium and silicon, probably deriving from concretions due to the permanence underground.

Figure 9 shows the distribution maps of the main elements of superficial patina and the bulk interface.
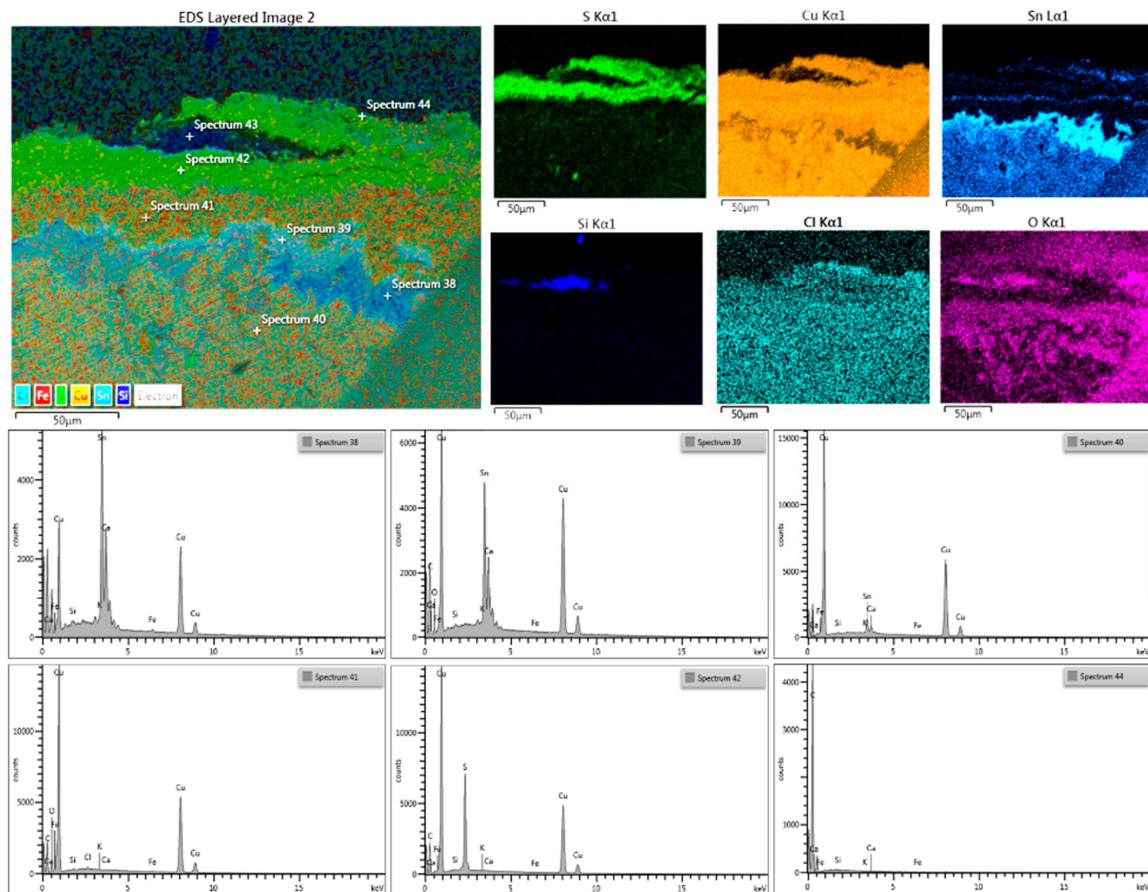

Figure 9. C2, above: EDX map of the front edge with oxidation patina and single elements distribution maps: Covellite (CuS) is lying on a cuprite (CuO) layer also on a cassiterite (SnO$_2$) thickening; the grains are well spaced and Fe and Si inclusions and Cl as the oxidizing agent are present as well. Below: EDX spectra of the point corresponding to different phases present in the cross-section.

The sample was embedded in resin, ground transversally, and then polished, producing a stratigraphic section that highlights the complete thickness of the lamina, a little less than an mm; the thicknesses of the patinas are visible (about 100 μm per side) with a curious, triple, and regular stratification in the face 2 (Figure 10). In a zone of face 1, there is a slight depression (a punching?) in which both the patina and other products of alteration of the metal alloy (reddish oxides) are observed. Near the two surfaces, close to the patina, there is inter-granular corrosion that highlights the grains of the metal alloy. The composition of the bulk bronze (inner grains, sp 40) is the richest in copper one (α-phase), whereas the material trapped among the inter granules is rich in SnO$_2$ (sp 38 and 39), while on the surface, the layers of copper patinas in the form of an oxide (sp 41) and sulfur compounds (sp 42) are seen, and there are traces of the organic substances of treatment after finding (synthetic resin, sp 44). The distribution map of the main elements in the cross-section and the reconstruction in arbitrary colors highlights the alternations of the layers and the relative elements. In particular, the layering of the covellite patinas is very regular and straight (Figure 10, the lower two green colored layers); it seems to be impossible to attribute them to a surface treatment or a particular contact with some unknown sulfur-rich substance.
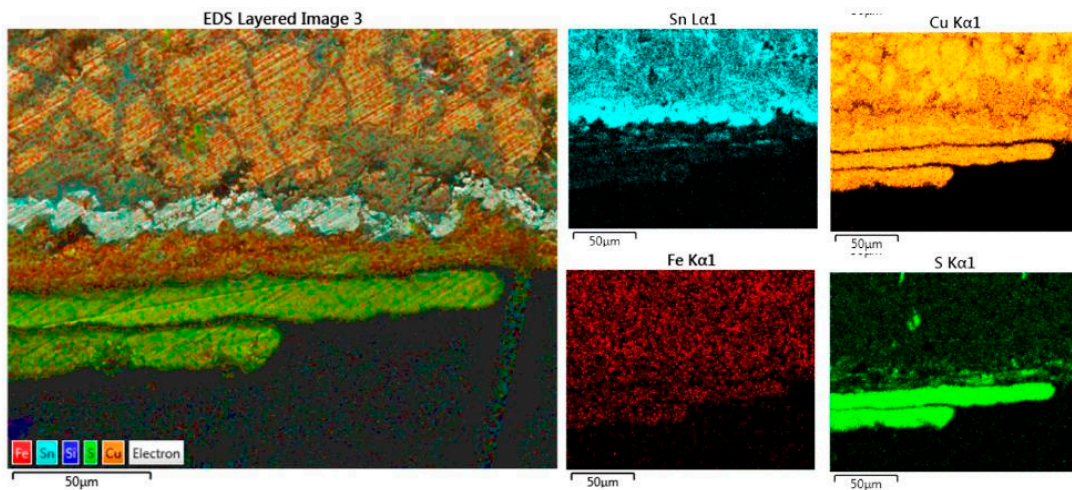
Figure 10. C2, EDX map of the rear edge with oxidation patina and the single-element distribution maps. In this detail, two regular CuS external layers are visible lying on a CuO layer also on an irregular jagged pure SnO_2 layer. The grains are deeply spaced and filled with tin oxidation products.

Micro-graphs of cross-sectioned patinas (darkfield observation) revealing the corrosion can assume different structures, which are in some cases stratified or, more often, a complex configuration where typically the green (more rarely blue) layer is composed by Cu (II)-containing minerals; the red areas are constituted by Cu (I) oxide (cuprite, Cu_2O), the dark areas are the surviving remains of the alloy, and the yellow-orange layer or pockets contain nantokite (CuCl). The fragment belonging to the bowl (Figure 11) shows a thick patina on both surfaces.
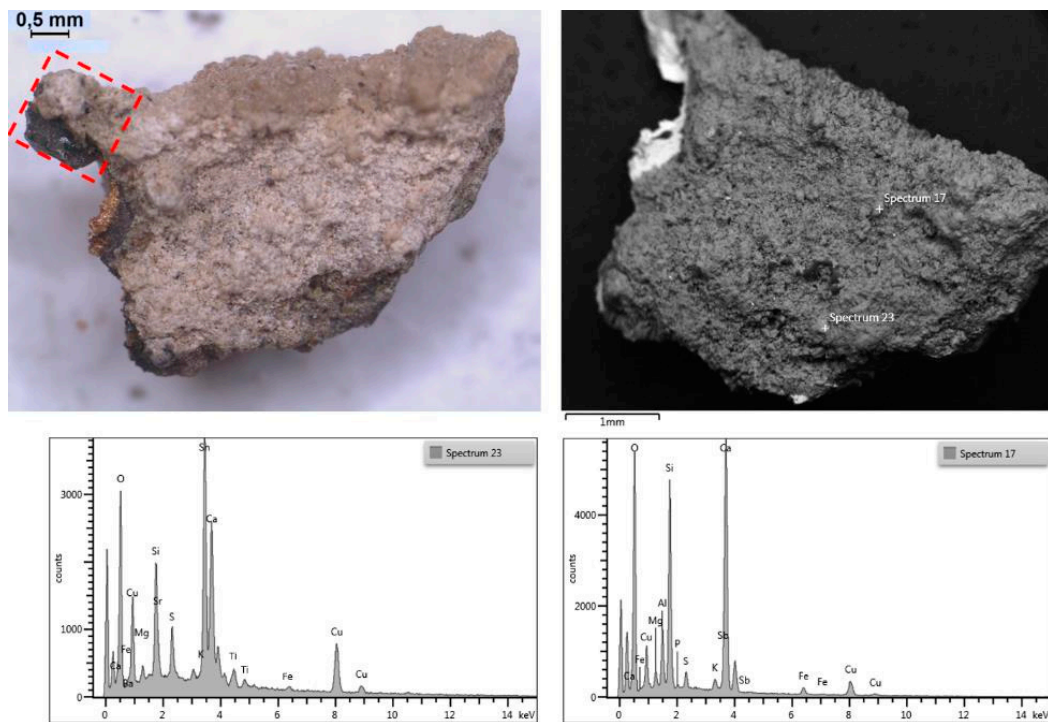

Figure 11. Macro photo of the C3 front surface (left) and the corresponding SEM/BSE image (right) of the thick patina; below, two EDS spectra of different superficial spots: many elements belonging to sediment and the corrosion product are present in addition to Sn and Copper. The red box corresponds to the micro fragment sampled and embedded in resin to realize the cross-section.

The cross-section of a micro-fragment taken from the sample allows us to appreciate the metal structure. It consists of a double pure bronze lamina (Figure 12), each one of different composition; taking into account that the greenish-yellow patina is deposited on the front side, the rear side, the lower in the photograph, appears lighter while the upper lamination has a warmer color; realistically, the color nuance corresponds respectively to a higher and a lower Sn content according to the color of raw metals: silver-color Sn and salmon-color Cu. The thicknesses are different because the upper sheet is about half of the lower one. The state of conservation is also notably different: the lower lamina appears much more fragmented and corroded and with more evident granulation than the upper lamina, which has remarkable compactness and appears perfectly adherent to the lower lamina; also, no noticeable granulation and oxidation phenomena are noted in the upper one.
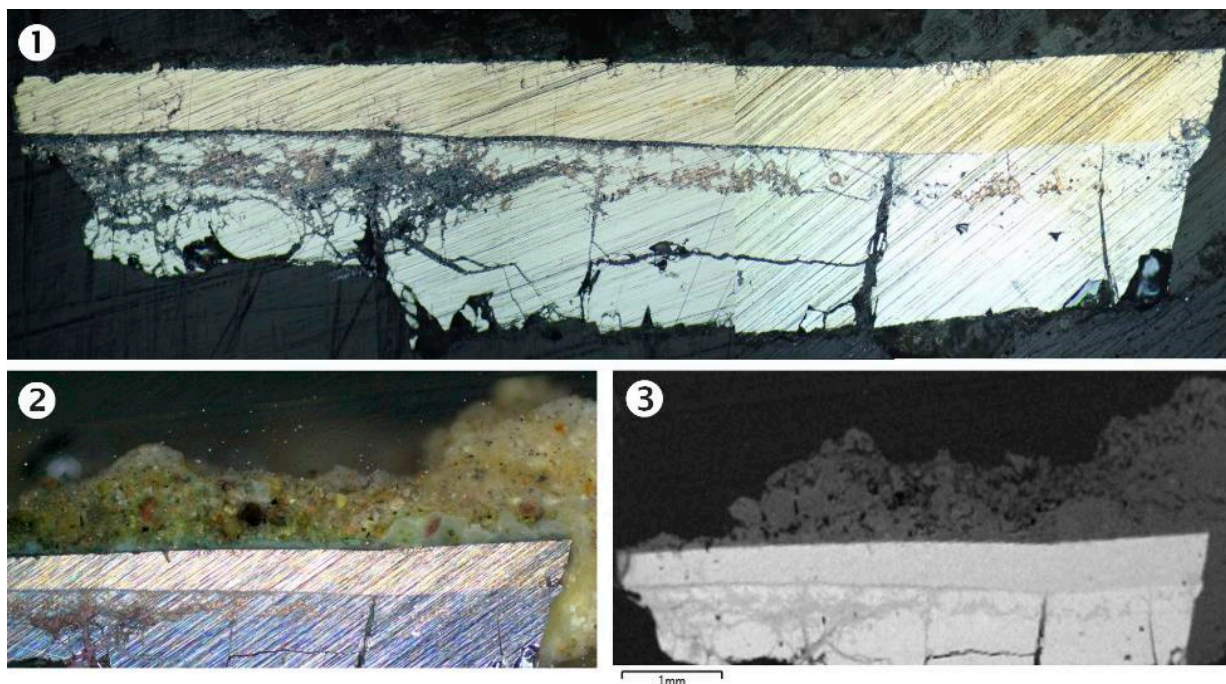

Figure 12. Microphotography of the cross-section of the bowl: (**1**) diffuse light, bright field, (**2**) dark field, (**3**) SEM/BSE image. There are visible two bronze plates intimately superimposed: the thinner has a golden color and is more compact, while the thicker is deeply cracked and corroded; BSE image reveals that the lower one is composed of the heaviest elements. A thick and irregular crust surrounds the whole laminated metal sheet (more appreciable in **2** and **3**). In between the metals (more on the left side of cross-section), a very thin and compact layer is perceptible separating the two foils.

The concremented patina appears thick and compact and has the typical colors of a sediment combined with products of oxidation of Sn (layered patina of white nebulous appearance adhering to the surface of the metal) and of mineral phases containing Cu (green, bluish products), both coming from bronze. Some charred fragments in an alumina–silicate matrix containing carbonates (calcite and dolomite) are present also, which is typical of the complexity of the excavated soil (Figure 13).

A curious and particular phenomenon lies in the interface between the two foils: a compact row of laminar crystals oriented in a direction orthogonal to the surface of the laminas divides the inner from the outer one: in the dark field image (true colors), the row of crystals looks pinkish in appearance. The EDS analysis shows that it is formed only from metallic copper; evidently, there is a reprecipitation by the reduction of native copper coming from the oxidation of the underlying bronze caused by the oxidation of Sn to SnO_2, which is adherent present as a grayish oxidized form in the lower lamina splits.
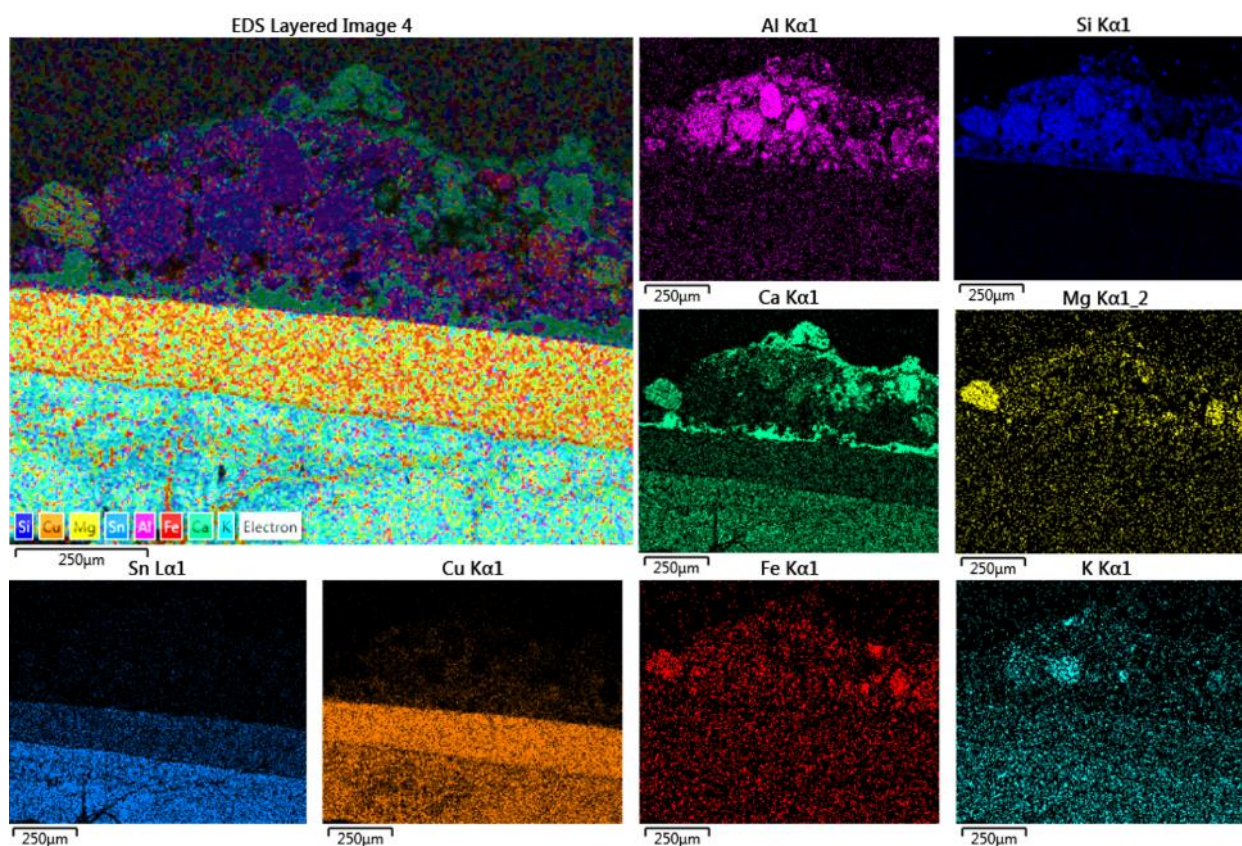
Figure 13. Close-up EDX reconstructed map of the elements forming the front crust; there is a plain layering among sediments and oxidation products of the alloy metals: alumina–silicates (feldspars), calcite (upper Ca layer), dolomite (Ca and Mg grains), and iron oxides. Warning: there is an overlap between $L\alpha_1$ Sn X-ray energy (3.44 KeV) and $K\alpha_1$ Ca one (3.69 KeV); thus, the patina covering the upper bronze foil is composed by SnO_2 and not erroneously attributed to Ca by the software.

It could be conceivable that the outer, finer lamina, richer in copper, caused an electrochemical effect on the thicker one, richer in tin, generating an overvoltage that reduced the copper from its oxides and oxidized the tin to dioxide (cassiterite); the latter migrated due to the lack of oxidized copper, while copper ions were discharged at the interface. The mechanism, considering the time of lying and the complexity of the environment that surrounded the find, can only be hypothesized and not demonstrated, although in other archaeological contexts, the presence of native copper in perfect octahedral crystals has already been encountered in the cavities of submerged Greek bronze [24].

The relative amount of the individual elements of the alloy is well represented in Figure 14: the more intense and pure the color, the greater the concentration. Copper (red color) is at the maximum concentration (purity) at the interface, in the upper sheet, it is more concentrated than in the lower one; the maximum concentration of tin, on the other hand, is in the oxide patina that delimits the lower foil (SnO_2, in blue) and in several oxidation diverticula that develop in it; then, in the two alloys, it is more concentrated in the latter than the upper one.
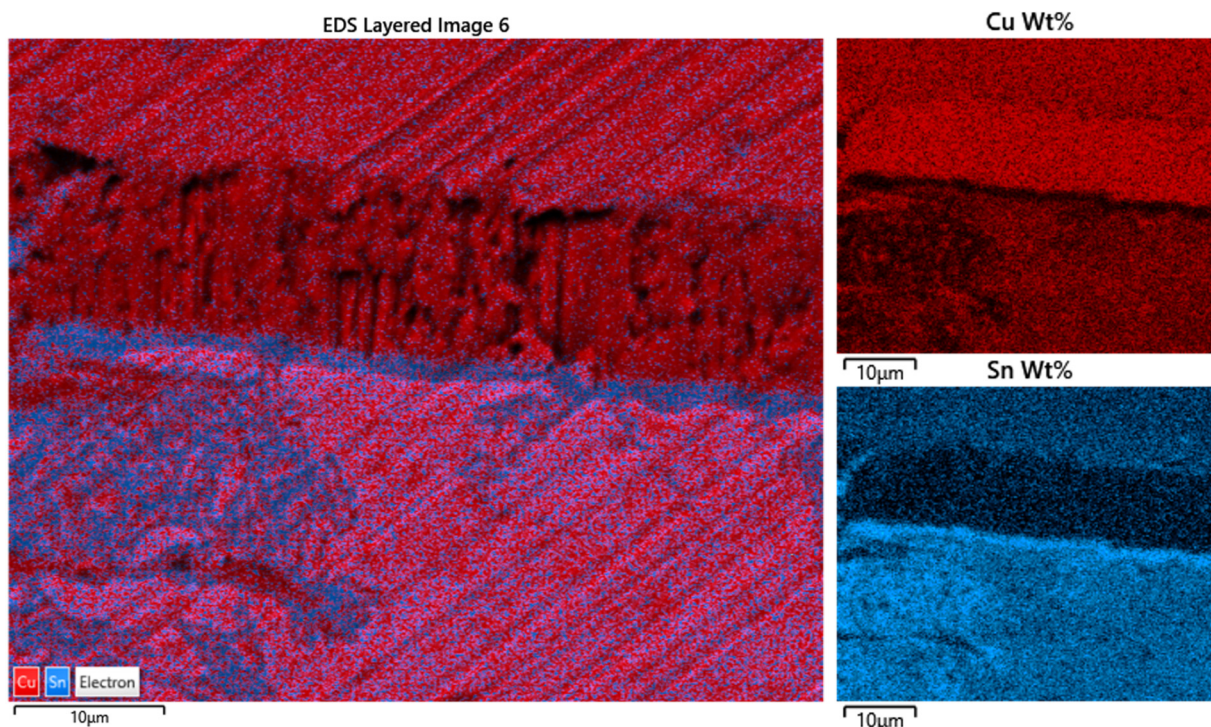
Figure 14. Detail of EDX reconstructed map of the alloy elements distribution at the interface between the two foils (red = Cu; blue = Sn); the reciprocal amount of the element concentration is appreciable. Copper is practically pure in the crystals between foils.

The EDX area analyses reveal the quantitative amount of the alloy elements: tin is present in the two laminas in different concentrations and at the boundary between the patina and the interface of the crystals; copper also follows this differentiated but reciprocally distribution: in the upper plate, the concentration is more than 90%, while in the other, it is around 65%. The figure shows the contact area between the two bronze plates with the interphase layer of pure copper (Figure 15). Spectra show the reciprocal amount of the elements: the more intense and pure the color, the greater the concentration, and some slight traces of sulfur and chlorine are present to indicate that the oxidation process is still occurring. Note the absence in the two sheets of any trace of other metals typically found in the bronze alloys (As, Sb, Pb, Zn).

The oxidation phenomena only concern the thicker foil with higher tin content (lower in the figure). Deep fractures of the lamina are recognized with the propagation of discontinuities even in micro-cracks starting from the upper lamina interface that expand and branch into the lower one. The growth and propagation of these slits is caused by the pressures generated by the oxides' crystallization produced in the electrochemical oxidative–reductive reactions in which the bronze sheet with the highest copper content acts as a cathode and the other, in which the most destructive corrosion phenomena occur, acts as an anode [22].

Figures 16 and 17 show a detail of the widespread situation of the lower foil, with the deep fractures in which cuprite crystals grow that widen them, until infiltrating humidity with solutions that concentrate and deposit tin oxides and insoluble mineral phases.
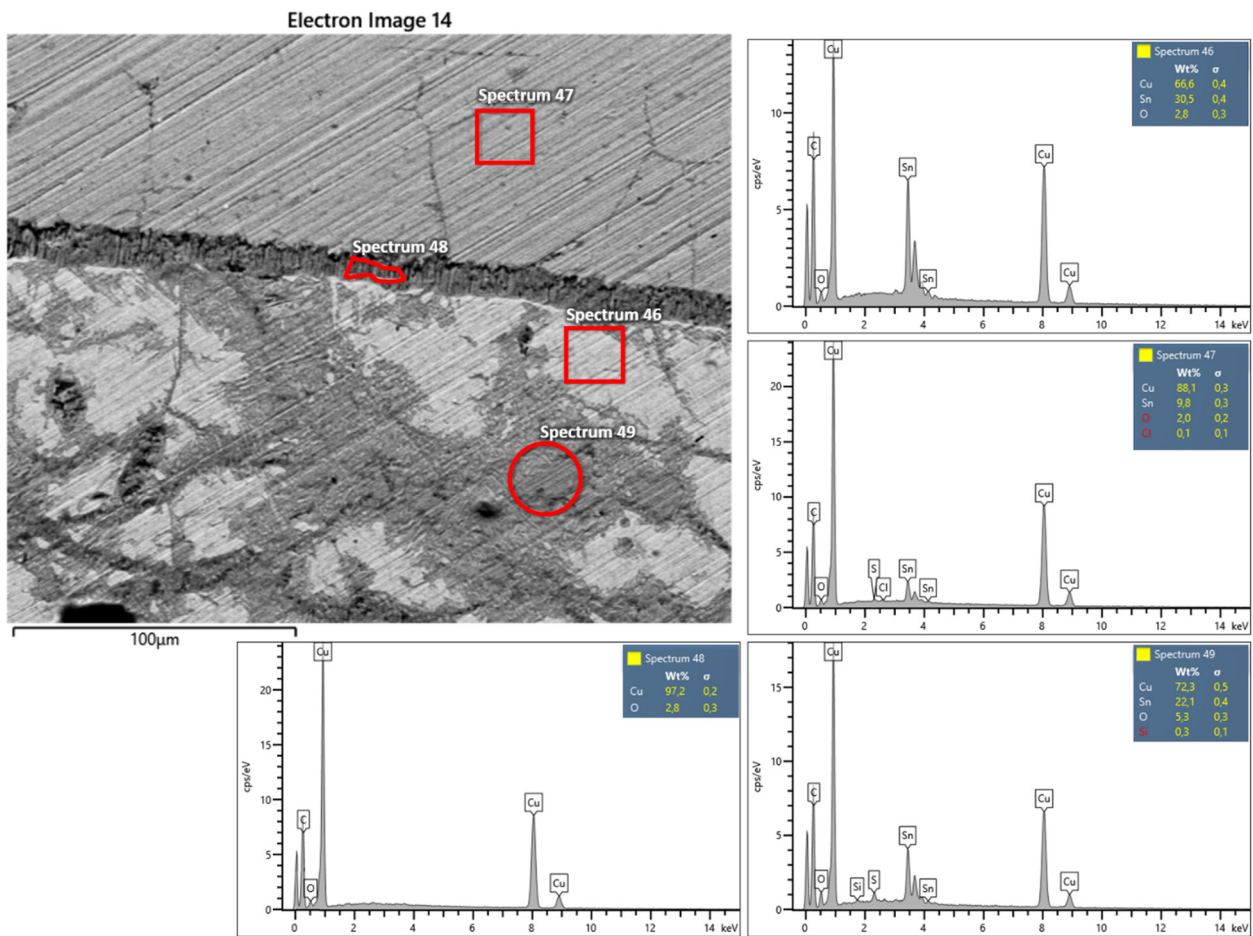
Figure 15. SEM/BSE details of the separation thin layer between the two bronze plates with the position of the EDX analyses spot and relative EDX spectra showing the composition of the alloys and the alteration products; sp 46 = grayish bronze (Cu ≈ 68%, Sn ≈ 31%), sp 47 = yellowish bronze (Cu ≈ 90%, Sn ≈ 10%), sp 48 = crystallization interphase (Cu ≈ 98%) and sp 49 = oxidation region. There is no presence of other elements composing the alloys; in addition, Cu, between metals, is practically neat.
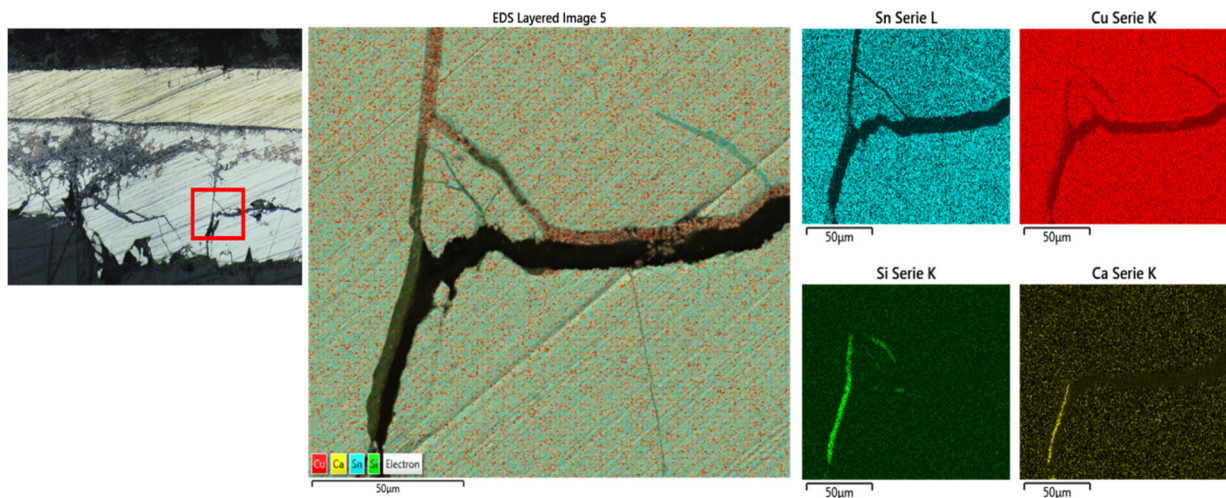

Figure 16. Cross-section and a detail of the analyzed area: reconstruction of the main elements EDX distribution map, and single EDX maps.
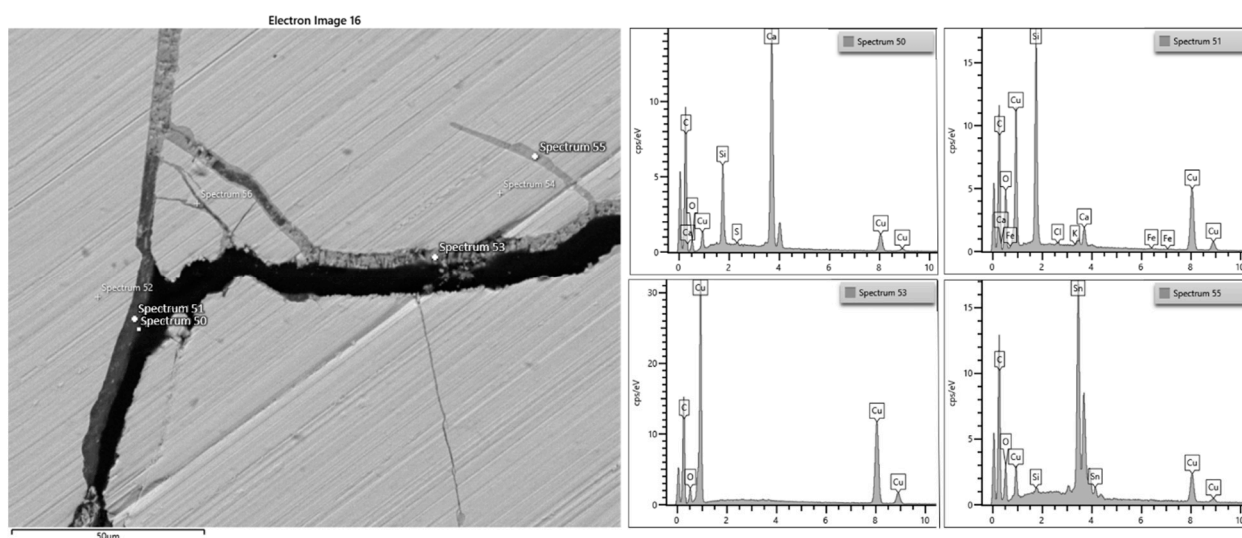
Figure 17. SEM/BSE image of the previous detail (Figure 16) in a lower plate with different points of EDX analyses. The cracks are filled by oxidation products (copper and tin dioxide, sp 53 and sp 55), and the mineral phases due to the burial environment are typically silicates (sp 51) and calcium carbonate (sp 50).

Certainly, the kinetics of these reactions was incredibly slow in the case of the exhibits presented, which was probably due to stationary conditions of humidity and soil composition. A long-term burial in the soil causes various corrosion morphologies in archaeological metals, from a thin corrosion layer to a completely corroded and mineralized artifact [9,25]. In recent years, valuable studies have been performed to characterize changes occurring in archaeological metals to understand their corrosion mechanism and morphology as well as conservation conditions [26–28].

4. Concluding Remarks

To characterize some archaeological bronze artifacts in Armenia, a micro-stratigraphic approach based on SEM-EDS and OM methods has been established. The bronze finds appear with the typical incrustations rich in alloy alteration compounds.

Copper-based artifacts include alloys with complex microstructures made up of distinct phases, which may vary according to the chemistry of the materials as well as the techniques used to fabricate the objects [27–31]. The preparation of ground and finely polished cross-section samples with uniform surface geometry facilitated dramatically SEM-EDS determination of the major element composition and the distribution of all present elements. Concentrations of copper and tin in the alloys were quantified by SEM-EDS: the type and the percentage of the alloy are same for samples 1 and 2, such as the aspect, the alloy grains, and the thickness, except for the covellite layers on the inner face of the sample 2. Concerning sample 3, it is constituted by two foils perfectly in contact but different in color, thickness, and composition; a particular redeposition of native copper is present between the lamina due to the electrochemical effect between the foil of different compositions (bimetallic galvanic corrosion). The micro-stratigraphic study helps us better understand the corrosion mechanism and morphology in bronze artifacts as well as their conservation conditions in the archaeological bronze collection of Yeghegnazor. The results determine that only two elements play the main role to form alloy composition in the samples: Cu and Sn. The tin content is variable from 7.75 to 13.56%. Other elements such as Ag, As, Fe, Ni, P, Pb, Sb, and Zn globally are lower than 1% in many samples and do not play an important role in the alloying process. They can be considered as impurities that may originate from mother stone ores.

Notes

[1]   Zeiss Axioplan 2, objectives from 2.5× to 50×, light sources: 100W halogen lamp and LED UV (λ = 360 nm) Zeiss "Colibri"; camera Canon EOS 1300D, 18 Mpx, software "Canon Image browser" with remote camera control.

References

1.   Bobokhyan, A.; Kunze, R.; Meliksetian, K.; Pernicka, E. Subartu XXXVIII At the Northern Frontier of Near Eastern Archaeology In Proceedings of the International Humboldt-Kolleg, Venice, Italic, 9–12 January 2013.
2.   Bobokhyan, A.; Meliksetian, K.; Gasparyan, B.; Avetisyan, P.; Chataigner, C.; Pernicka, E. *Transition to Extractive Metallurgy and Social Transformation in Armenia at the End of the Stone Age, Stone Age of Armenia a Guide-Book to the Stone Age Archaeology in the Republic of Armenia*; Boris Gasparyan and Makoto Arimura: Kanazawa, Japan, 2014.
3.   Mazzeo, R.; Prati, S.; Quaranta, M.; Sciuto, G. An overview of analytical techniques and methods for the study and preservation of artistic and archaeological bronzes. *Mediterr. Archaeol. Archaeom.* **2012**, *12*, 261–271.
4.   Bernard, M.; Joiret, S. Understanding corrosion of ancient metals for the conservation of cultural heritage. *Electrochim. Acta* **2009**, *54*, 5199–5205. [CrossRef]
5.   Bertolotti, G.; Bersani, D.; Lottici, P.P.; Alesiani, M.; Malcherek, T.; Schlüter, J. Micro-Raman study of copper hydroxychlorides and other corrosion products of bronze samples mimicking archaeological coins. *Anal. Bioanal. Chem.* **2011**, *402*, 1451–1457. [CrossRef] [PubMed]
6.   Doménech, A.; Doménech-Carbó, M.T.; Pasies, T.; Bouzas, M.D.C. Modeling Corrosion of Archaeological Silver-Copper Coins Using the Voltammetry of Immobilized Particles. *Electroanalysis* **2012**, *24*, 1945–1955. [CrossRef]
7.   Rizzo, F.; Cirrone, G.P.; Cuttone, G.; Esposito, A.; Garraffo, S.; Pappalardo, G.; Pappalardo, L.; Romano, F.P.; Russo, S. Non-destructive determination of the silver content in Roman coins (nummi), dated to 308–311 A.D., by the combined use of PIXE-alpha, XRF and DPAA techniques. *Microchem. J.* **2011**, *97*, 286–290. [CrossRef]
8.   Robbiola, L.; Blengino, J.-M.; Fiaud, C. Morphology and mechanisms of formation of natural patinas on archaeological Cu–Sn alloys. *Corros. Sci.* **1998**, *40*, 2083–2111. [CrossRef]
9.   Ingo, G.; de Caro, T.; Riccucci, C.; Khosroff, S. Uncommon corrosion phenomena of archaeological bronze alloys. *Appl. Phys. A* **2006**, *83*, 581–588. [CrossRef]
10.   Scott, D.A. *Copper and Bronze in Art: Corrosion, Colorants and Conservation*; Getty Conservation Institute Publications: Los Angeles, CA, USA, 2002.
11.   Scott, D.A. An examination of the patina and corrosion morphology of some Roman bronzes. *J. Am. Inst. Conserv.* **1994**, *33*, 1–23. [CrossRef]
12.   Martirosyan, A. *Armenia in Iron and Bronze Ages*; University Publisher: Yerevan, Armenia, 1964; pp. 245–250.
13.   Esayan, C.A.; Khnkikyan, O.C. Discovery of Biainil rests at Yegheghnadzor. *Banber Yerevani Hamals.* **1990**, *3*, 37–43.
14.   Manukyan, S. Bronze belts of Lchashen-Metsamor culture in the sculptures of the same period. *Arvestagir* **2015**.
15.   Meliksetian, K.; Pernicka, E. Geochemical characterisation of Armenian Early Bronze Age metal artefacts and their relation to copper ores. Hansen, S., Hauptmann, A., Motzenbäcker, I., Pernicka, E., Eds.; Von Majkop bis Trialeti. Gewinnung und Verbreitung von Metallen und Obsidian in Kaukasien im 4.-2. In Proceedings of the Jt. v. Chr. Beiträge des Internationalen Symposiums, Berlin, Germany, 1–3 June 2006.
16.   Meliksetian, K.; Pernicka, E.; Badalyan, R.; Avetisyan, P. Geochemical characterisation of Armenian early bronze age metal artefacts and their relation to copper ores. In Proceedings of the International Conference on Archaeometallurgy in Europe, Milan, Italy, 24–26 September 2003; Volume 1.

17. Meliksetian, K.; Pernicka, E.; Avetisyan, P.; Simonyan, H. Chemical and lead isotope characterisation of Middle Bronze Age bronzes and some Iron Age antimony objects (Armenia). In Proceedings of the International conference on Archaeometallurgy in Europe, Milan, Italy, 24–26 September 2003; Volume 2.
18. Meliksetian, K.; Kraus, S.; Pernicka, E.; Avetissyan PDevejian, S.; Petrosyan, L. *Metallurgy of Prehistoric Armenia, Anatolian Metal V*; Herausgeber: Ünsal Yalçın, Bochum, 2011.
19. Lalli, C.; Lanterna, G.; Pinna, D.; Porcinai, S.; Rizzi, M.; Tosini, I. Indagini diagnostiche. In *Apoxyomenos, the Athlete of Croatia*; Michellucci Curator, Giunti: Florence, Italy, 2006; pp. 117–118.
20. Oudbashi, O.; Hassanpour, A.; Davami, P. Investigation on corrosion stratigraphy and morphology in some Iron Age bronze alloys vessels by OM, XRD and SEM–EDS methods. *Appl. Phys. A Mater. Sci. Process.* **2016**, *122*, 262. [CrossRef]
21. Oudbashi, O.; Wanhill, R. Long-term embrittlement of ancient copper and silver alloys. *Heritage* **2021**, *4*, 2287–2319. [CrossRef]
22. Oddy, W.A.; Meeks, N.D. Unusual phenomena in the corrosion of ancient bronzes. In *Science and Technologies, IIC Washington Congress*; Brommelle, N.S., Thomas, G., Eds.; Taylor & Francis: Boca Raton, FL, USA, 1982; pp. 119–124.
23. Scott, D.A. Corroded microstructures. In *Metallography and Microstructure of Ancient and Historic Metals*; Paul Getty Conservation Institute: Malibu, CA, USA, 1991; pp. 43–48.
24. Robbiola, L.; Fiaud, C. Corrosion structures of long-term burial Cu-Sn alloys. In *Influence of the Selective Dissolution of Copper. Int. Symp. "Copper and Copper Alloys Oxidation"*; Mém. Et. Scien. Rev. Métallurgie: Paris, France, 1992; pp. 157–162.
25. Michelucci, M. Archaeological and archaeometric data in the study of the athlete of Croatia. In Proceedings of the Science for Cultural Heritage: Technological Innovation and Case Studies in Marine and Land Archaeology in the Adriatic Region and Inland: VII International Conference on Science, Arts and Culture, Veli Lošinj, Croatia, 28–31 August 2007.
26. Robbiola, L.; Fiaud, C.; Harch, A. Characterization of passive layers of bronze patinas (Cu-Sn alloys) in relation with the tin content in the alloy. In *Modifications of Passive Films, Europ. Fed. of Corrosion*; Marcus, P., Baroux, B., Keddam, M., Eds.; The Institute of Materials: London, UK, 1994; pp. 150–154. ISBN 0-901716-52-9.
27. Sandu, I.; Ursulescu, N.; Sandu, I.G.; Bounegru, O.; Sandu, I.C.A.; Alexandru, A. Pedological stratification effect of corrosion and contamination products on Byzantine bronze artefacts. *Corros. Eng. Sci. Technol.* **2008**, *43*, 256–267. [CrossRef]
28. Scott, D.A. Corrosion and Environment. In *Copper and Bronze in Art*; Paul Getty Conservation Institute: Malibu, CA, USA, 2002; pp. 10–80.
29. Selwyn, L.S. Corrosion of metal artefacts in buried environments. In *ASM Handbook. Vol. 13C. Corrosion: Environments and Industries*; National Bureau of Standards (NBS): Washington, DC, USA, 2006; pp. 306–322.
30. Cushing, D. *Principles of Corrosion Applicable to Ancient Metals and Methods of Identifying Corrosion Products*; Application of Science in the Examination of Works of Art: Boston, MA, USA, 1967; pp. 53–65.
31. Wadsak, M.; Constantinides, I.; Vittiglio, G.; Adriaens, A.; Janssens, K.; Schreiner, M.; Adams, F.C.; Brunella, P.; Wuttmann, M. Multianalytical study of patina formed on archaeological metal objects from Bliesbruck-Reinheim. *Microchim. Acta* **2000**, *133*, 59–164. [CrossRef]